Chemistry–A European Journal

Supporting Information

# Cobaloxime Complex Salts: Synthesis, Patterning on Carbon Nanomembranes and Heterogeneous Hydrogen Evolution Studies

Chemistry–A European Journal

Supporting Information

Cobaloxime Complex Salts: Synthesis, Patterning on Carbon Nanomembranes and Heterogeneous Hydrogen Evolution Studies

## Author Contributions

E.O. Data curation:Equal; Investigation:Lead; Writing – original draft:Supporting
A.-L.G. Investigation:Equal
J.K. Investigation:Supporting
M.K. Investigation:Supporting
J.R. Investigation:Supporting
S.W. Investigation:Supporting
T.U. Investigation:Supporting; Supervision:Supporting
A.M. Investigation:Supporting
L.P. Investigation:Supporting
R.L. Investigation:Supporting
P.U. Software:Supporting
U.K. Funding acquisition:Supporting; Supervision:Supporting
S.R. Conceptualization:Supporting; Funding acquisition:Supporting; Supervision:Supporting
A.K. Data curation:Supporting; Supervision:Supporting
A.T. Conceptualization:Supporting; Funding acquisition:Supporting; Supervision:Supporting
M.v. Conceptualization:Lead; Funding acquisition:Equal; Project administration:Lead; Supervision:Lead; Writing – original draft:Lead; Writing – review & editing:Lead
C.K. Conceptualization:Lead; Funding acquisition:Equal; Project administration:Lead; Supervision:Lead; Writing – original draft:Lead; Writing – review & editing:Lead

Supporting Information

# Cobaloxime complex salts: synthesis, patterning on carbon nanomembranes and heterogeneous hydrogen evolution studies

Eva Oswald,[a],† Anna-Laurine Gaus,[b],† Julian Kund,[a] Maria Küllmer,[c] Jan Romer,[a] Simon Weizenegger,[b] Tobias Ullrich,[d] Alexander K. Mengele,[e] Lydia Petermann,[e] Robert Leiter,[f] Patrick R. Unwin,[g] Ute Kaiser,[f] Sven Rau,[e] Axel Kahnt,[h] Andrey Turchanin,[c] Max von Delius*[b] and Christine Kranz*[a]

[a] E. Oswald, J. Kund, J. Romer, Prof. Dr. C. Kranz
Institute of Analytical and Bioanalytical Chemistry
Albert-Einstein-Allee 11, 89081 Ulm, Germany
E-mail: christine.kranz@uni-ulm.de

[b] A.-L. Gaus, S. Weizenegger, Prof. Dr. M. von Delius
Institute of Organic Chemistry I,
Ulm University
Albert-Einstein-Allee 11, 89081 Ulm, Germany
E-mail: max.vondelius@uni-ulm.de

[c] M. Küllmer, Prof. Dr. A. Turchanin
Institute of Physical Chemistry
Friedrich Schiller University Jena
Lessingstrasse 10, 07743 Jena, Germany

[d] T. Ullrich
Department of Chemistry and Pharmacy
FAU Erlangen-Nürnberg
Egerlandstrasse 3, 91058 Erlangen, Germany

[e] A. K. Mengele, Dr. L. Petermann, Prof. Dr. A. Rau
Institute of Inorganic Chemistry I
Ulm University
Albert-Einstein-Allee 11, 89081 Ulm, Germany

[f] R. Leiter, Prof. Dr. U. Kaiser
Central Facility Electron Microscopy, Materials Science Electron Microscopy
Ulm University
Albert-Einstein-Allee 11, 89081 Ulm, Germany

[g] Prof. Dr. P. R. Unwin
Department of Chemistry, University of Warwick
Gibbet Hill Road, Coventry, CV4 7AL, United Kingdom

[h] Dr. A. Kahnt
Leibniz-Institute of Surface Engineering (IOM),
Permoserstrasse 15, 04318 Leipzig, Germany

† These authors contributed equally

**Contents**

## 1. General Experimental Section

All commercially available reagents for syntheses were purchased from Sigma Aldrich, Alfa Aesar, Acros Organics or TCI and were used without further purification. For studies on CNM support, acetonitrile (≥99.9%), L-(+)-ascorbic acid (99.0-100.5%) and sodium hydroxide (≥97%) were purchased from VWR Chemicals, Darmstadt, Germany. 1,1'-Ferrocendimethanol (98%) was purchased from Acros Organics, Fair Lawn, USA. Potassium tetrachloropalladate(II) (99.99%) was purchased from Alfa Aesar, Thermo Fisher GmbH, Kandel, Germany. Potassium chloride was purchased from Merck KGaA, Darmstadt, Germany. $[Ru(tbbpy)_2(mmip)]Cl_3$ was synthesized at the Institute of Inorganic Chemistry, Ulm University.[S1] High purity water (18.1 MΩcm) from ELGA LabWater, High Wycombe, United Kingdom was used to prepare the solutions. Ag (0.15 mm), Au/Ni microwires (0.025 mm) and Pt (0.4 mm) wires were purchased from Goodfellow, Bad Nauheim, Germany. NBPT (99%) was obtained from Taros and sublimated before use. DMF for NBPT SAM preparation was purchased from VWR (anhydrous, < 0.005% $H_2O$).

NMR spectra were recorded on Bruker Avance (Neo) 400 ($^1$H: 400 MHz) spectrometers at room temperature and referenced to the residual solvent peak ($^1$H: $CDCl_3$, 7.26 ppm; $CD_3CN$: 1.94 ppm; $^{13}$C: DMF-d7: 163.15 ppm; $CD_3CN$: 118.26 ppm). Coupling constants (*J*) are denoted in Hz and chemical shifts (δ) in ppm. Mass spectra were obtained on an Agilent 6546 QTOF instrument (HRMS-ESI, solvent: acetonitrile). Hydrogen evolution was quantified by headspace GC analysis on a Bruker Scion GC with a thermal conductivity detector 15 (column: Mol sieve 5Å 75 m x 0.53 mm I.D., oven temp. 70 °C, flow rate 30.0 ml/min, detector temp. 200 °C) with argon as a carrier gas. A GC calibration curve was obtained by injecting specific amounts of hydrogen. For the photocatalytic experiments, 100 µL of the headspace were injected and the amount of hydrogen was determined with the help of the calibration curve.

HER experiments were carried out in 21 mL Schlenk-tubes filled with 7 mL solvent, capped with rubber septa. All hydrogen evolution reaction studies were carried out in anhydrous solvents stored under inert atmosphere. The temperature was held constant by a custom-made air-cooling setup (25 °C). Irradiation of the samples was performed utilizing two LED sticks ($\lambda_{max}$ = 475 nm ± 5 nm, power density at the sample ca. 45 mW/cm$^2$, custom-made at Ulm University). Both sticks were placed on opposite sides of the reaction vessel at a distance of approximately 0.5 cm.

In a typical experiment, the Schlenk tube was filled with catalyst (0.043 mmol/L), photosensitizer (0.043 mmol/L), acetone (7 mL), triethylamine (1000 equiv.) and triethylammonium tetrafluoroborate[S2] (1000 equiv.) in a nitrogen-filled glovebox. All stock solutions were freshly prepared right before filling the Schlenk tubes.

Electrochemical data were recorded by cyclic voltammetry using a Bio-logic, VSP300 Research potentiostat in combination with a three-electrode system. The working electrode consisted of a platinum electrode, the counter electrode was a platinum wire, while a sliver wire was used as the reference electrode. The measurements were carried out in argon saturated acetonitrile. Tetrabutylammonium hexafluorophosphate (0.1 M) was used as electrolyte salt. A scan rate of 50 mV / s was selected. All potentials are referenced to ferrocenium/ferrocene ($Fc^+$/Fc).

Crystals suitable for X-ray crystallography were mounted using a MicroLoop and perfluoropolyalkylether (viscosity 1800 cSt). X-ray diffraction intensity data were measured at 150 K with a SuperNova (Dual Source) diffractometer, equipped with an ATLAS detector from Agilent Technologies, using graphite-monochromated Mo-$K_\alpha$ irradiation. Using Olex2,[S3] the structure was solved with the SHELXS[S4] structure solution program using Direct Methods and refined with the SHELXL[S5] refinement package using Least Squares minimization. The hydrogen atoms were included at calculated positions with fixed thermal parameters. All non-hydrogen atoms were refined anisotropically. MERCURY was used for structural representations.[S6]

A 5500 AFM/SPM from Keysight Technologies (Tempe, AZ, USA) was used for all AFM measurements using the PicoView 1.20 software. All measurements were performed in contact mode in air with silicon nitride probes (ORC-8, Bruker AFM probes, CA, USA). Images were recorded with a scan speed of 0.5 ln s-1.

SEM imaging was obtained with Helios Nanolab 600 FIB/SEM (ThermoFisher, FEI, Eindhoven, Netherlands) operating at 1 – 3 kV and beam currents of 86 pA, respectively 170 pA by using the in-lens detector (immersion mode) of the instrument.

Scanning Transmission Electron Microscopy (STEM) (ThermoFisher Talos F200X G2 STEM microscope) operated in STEM mode for simultaneous acquisition of high-angle annular dark field (HAADF) images and spatially resolved energy dispersive x-ray (EDX) spectra was used. Those spectra were background-subtracted and used to generate elemental maps.

## 2. Synthesis Overview

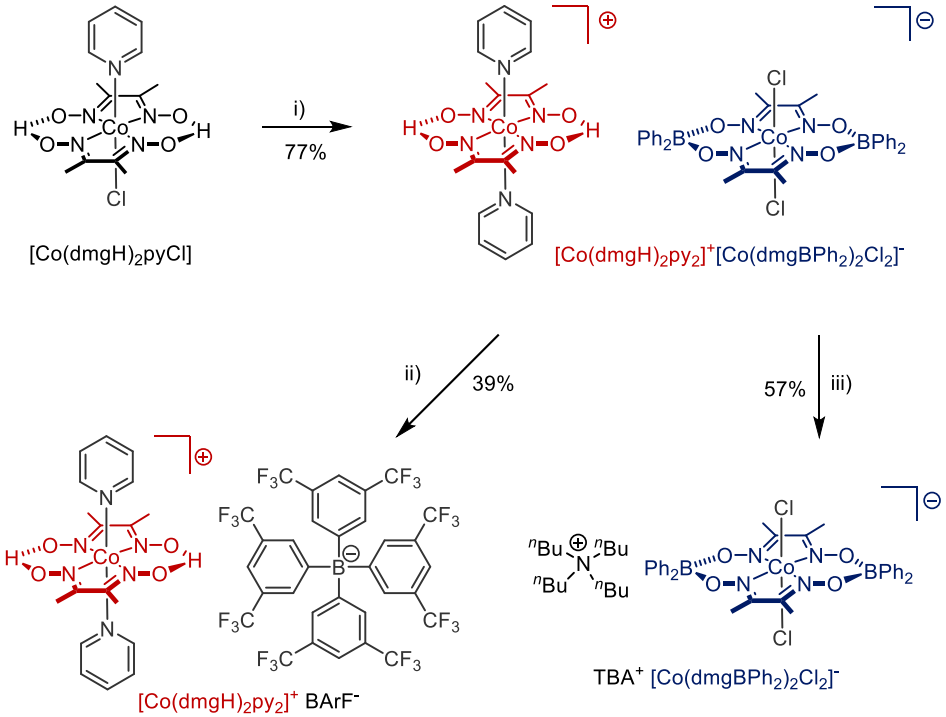


**Scheme S1.** Reaction conditions: (i) $BPh_3$, dry MeCN, r.t., 6 h; (ii) $NaBAr^F$, $CHCl_3$, r.t., 20 min; (iii) washed with aqueous TBACl solution and $CHCl_3$; All yields are isolated yields.

## 3. Synthetic Procedures and Characterization Data

### 3.1. Synthesis of $[Co(dmgH)_2(py)_2]^+[Co(dmgBPh_2)_2Cl_2]^-$

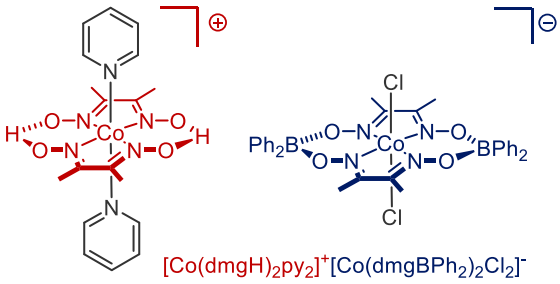


$[Co(dmgH)_2(py)_2]^+[Co(dmgBPh_2)_2Cl_2]^-$ was prepared by stirring $[Co(dmgH)_2(py)Cl]$ (200 mg) at room temperature with triphenylborane (242 mg) in anhydrous acetonitrile (9.0 mL). The reaction mixture was stirred for 5 h at room temperature. The product precipitated from solution. The precipitate was collected and washed with $Et_2O$ (4.0 mL), ethanol (4.0 mL), and $H_2O$ (2.0 mL), to yield pure $[Co(dmgH)_2(py)_2]^+[Co(dmgBPh_2)_2Cl_2]^-$ as a brown solid (220 mg, 77%). Please note that yields were found to vary depending on the batch of $[Co(dmgH)_2(py)Cl]$ starting material (purchased from Sigma-Aldrich).

$^1$H-NMR (400 MHz, acetonitrile-$d_3$): δ = 8.24 - 8.23 (m, 4H, $CH_{py}$), 7.89 - 7.85 (m, 2H, $CH_{py}$), 7.43 - 7.37 (m, 12H, $CH_{py}$ + $CH_{ph}$), 7.06 - 7.02 (m, 8H, $CH_{ph}$), 6.95 - 6.91 (t, 4H, $CH_{ph}$), 2.73 (s, 12H, $CH_3$), 2.24 (s, 12H, $CH_3$) ppm.

$^{13}$C-NMR (400 MHz, 333 K, DMF-d7): δ = 158.0, 157.2, 152.2, 141.7, 133.1, 133.0, 127.9, 127.2, 125.4, 14.0, 13.8 ppm.

HR MS (ESI): positive mode: Calculated for $C_{18}H_{24}CoN_6O_4$: 447.1191. Found: 447.11932 m/z
negative mode: Calculated for $C_{32}H_{32}B_2Cl_2CoN_4O_4$: 687.1319. Found: 687.13267 m/z

(Decomposition temperature: 238 °C – 250 °C. Decomposition occurs before melting.)

### 3.2. Synthesis of $[Co(dmgH)_2(py)_2]^+BArF^-$

$[Co(dmgH)_2(py)_2]^+[Co(dmgBPh_2)_2Cl_2]^-$ (20 mg) was suspended in $CHCl_3$ (6 mL) and NaBArF (22 mg) was added. The mixture was stirred for 20 min and quenched with $H_2O$ (7 mL). The phases were separated, the organic phase was washed with $H_2O$ (2 x 10 mL) and dried over $MgSO_4$. The solvent was removed under reduced pressure. The resulting solid was washed with cold $Et_2O$ yielding pure $[Co(dmgH)_2(py)_2]^+$ $BarF^-$ as a beige orange solid (9 mg, 39%).

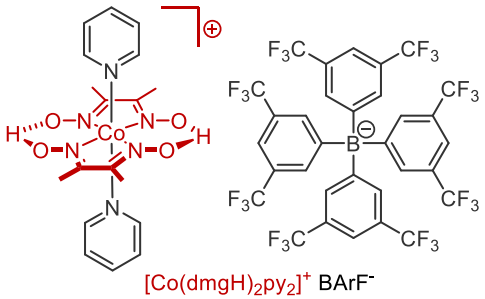


$[Co(dmgH)_2py_2]^+$ $BArF^-$

$^1$H-NMR (400 MHz, acetonitrile-$d_3$): δ = 8.25 - 8.23 (m, 4H, $CH_{py}$), 7.89 - 7.85 (m, 2H, $CH_{py}$), 7.69 - 7.66 (m, 12H, $CH_{BArF}$), 7.41 - 7.37 (m, 4H, $CH_{py}$), 2.24 (s, 12H, $CH_3$) ppm.

$^{13}$C-NMR (400 MHz, 298 K, acetonitrile-$d_3$): δ = 163.3 - 161.8 ($CF_3$), 157.5, 152.1, 141.2, 135.6, 127.5, 126.8, 124.1, 13.6 ppm.

HR MS (ESI): positive mode: Calculated for $C_{18}H_{24}CoN_6O_4$: 447.1191. Found: 447.11921 m/z
negative mode: Calculated for $C_{32}H_{12}BF_{24}$: 863.0649. Found: 863.06543 m/z.

### 3.3. Synthesis of $TBA^+[Co(dmgBPh_2)_2Cl_2]^-$

$[Co(dmgH)_2(py)_2]^+[Co(dmgBPh_2)_2Cl_2]^-$ (20 mg) was suspended in $CHCl_3$ (20 mL) and washed with an aqueous tetrabutyl ammonium hydroxide solution (0.1 M; 3 x 30 mL). The phases were separated, the organic phase was washed with $H_2O$ (4 x 20 mL) to remove excess $TBA^+$ and dried over $MgSO_4$. The solvent was removed under reduced pressure yielding pure $TBA^+[Co(dmgBPh_2)_2Cl_2]^-$ as a light beige solid (10 mg, 57%).

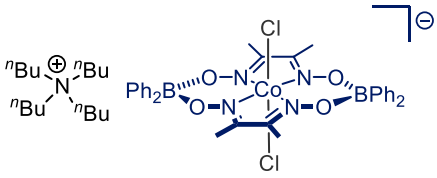


$TBA^+$ $[Co(dmgBPh_2)_2Cl_2]^-$

$^1$H NMR (400 MHz, acetonitrile-$d_3$): δ = 7.43 - 7.41 (m, 8H, $CH_{ph}$), 7.06 - 7.02 (m, 8H, $CH_{ph}$), 6.95 – 6.91 (m, 4H, $CH_{ph}$), 3.09 - 3.04 (m, 8H, $CH_2$), 2.73 (s, 12H, $CH_3$), 1.62 -1.55 (m, 8H, $CH_2$), 1.39 – 1.27 (m, 8H, $CH_2$), 0.98 – 0.95 (m, 12H, $CH_3$) ppm.

$^{13}$C-NMR (400 MHz, 298 K, acetonitrile-$d_3$): δ = 157.9, 132.3, 132.1, 127.4, 125.5, 59.3, 24.3, 20.3, 14.1, 13.7.

HR MS (ESI): positive mode: Calculated for $C_{16}H_{36}N$: 242.2848. Found: 242.28548 m/z.
negative mode: Calculated for $C_{32}H_{32}B_2Cl_2CoN_4O_4$: 687.1319. Found: 687.13299 m/z.

## 4. Photocatalytic Hydrogen Evolution Reactions

### 4.1. Sample preparation

Depending on the solubility of the synthesized catalysts in acetone, different preparation methods were used. Stock solution of photosensitizer (0.43 mmol/L) and the proton source $HNEt_3^+$ $BF_4^-$ (0.23 mol/L) each in acetone were prepared on the measurement day.

Method A

Because of their good solubility, respectively 5.6 mg $[Co(dmgH)_2(py)_2]^+$ $BArF^-$ or 4.0 mg $TBA^+$ $[Co(dmgBPh_2)_2Cl_2]^-$ were dissolved in acetone (4.3 mmol/L). 0.7 mL of the catalyst in acetone, 0.7 mL of the photosensitizer stock solution (0.43 mmol/L), 0.043 mL of $Et_3N$, 1.4 mL of $HNEt_3^+$ $BF_4^-$ (0.23 mol/L) and 4.2 mL of acetone were added to each reaction tube in a nitrogen-filled glovebox.

Method B

Stock solutions of catalysts with lower solubility like $[Co(dmgH)_2(py)Cl]$ (0.06 mmol/L) and $[Co(dmgH)_2(py)_2]^+$ $[Co(dmgBPh_2)_2Cl_2]^-$ (0.15 mmol/L) were prepared in acetonitrile. After adding the right amount of catalyst to the Schlenk tube, the solvent was removed under reduced pressure and dried for additional 18 h at the vacuum pump. 0.7 mL of the photosensitizer stock solution (0.43 mmol/L), 0.043 mL of $Et_3N$, 1.4 mL of $HNEt_3^+$ $BF_4^-$ (0.23 mol/L) and 4.9 mL of acetone were added to the tubes already containing dry catalyst in a nitrogen-filled glovebox. The reaction mixtures were homogenized in the ultrasonic bath for 30 sec. before starting the measurements.

### 4.2. Light Source

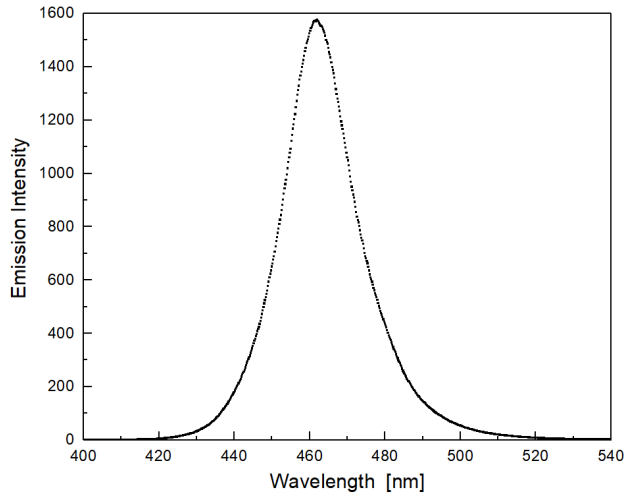


**Table S1: E**mission maxima of LED lamps used in this study

| Entry | wavelength at maximum emission intensity [λ] |
|---|---|
| 1 | 462.2 |
| 2 | 461.0 |
| 3 | 462.0 |
| 4 | 461.8 |
| 5 | 462.4 |
| 6 | 463.0 |
| **Average** | 462.1 |
| **Std. deviation** | 0.6 |

## 4.3. Overview on HER Experiments

Measurements were carried out every hour during illumination. Each sample was measured before the start of the illumination giving a measurement point at 0 h.

[catalyst]: 0.043 mmol/L; [PS]: 0.043 mmol/L; [$e^-$ donor]: 43 mmol/L

**Table S2:** results of investigated HER

| Entry | Catalyst | Photo-sensitizer | $e^-$ do-nor | Solvent | Light source | Atmos-phere | TON[a] | TOF[b] |
|---|---|---|---|---|---|---|---|---|
| 1 | $[Co(dmgH)_2(py)Cl]$ | $Ru(bpy)_3^{2+}$ | TEA | acetone | LED, 460 nm | $N_2$ | 35 (± 2) | 18 (± 2) |
| 2 | $[Co(dmgH)_2(py)_2]^+$ $[Co(dmgBPh_2)_2Cl_2]^-$ | $Ru(bpy)_3^{2+}$ | TEA | acetone | LED, 460 nm | $N_2$ | 61 (± 3) | 8 (± 1) |
| 3 | $[Co(dmgH)_2(py)_2]^+$ $BArF^-$ | $Ru(bpy)_3^{2+}$ | TEA | acetone | LED, 460 nm | $N_2$ | 65 (± 2) | 19 (± 0) |
| 4 | $TBA^+$ $[Co(dmgBPh_2)_2Cl_2]^-$ | $Ru(bpy)_3^{2+}$ | TEA | acetone | LED, 460 nm | $N_2$ | 56 (± 3) | 23 (± 2) |

[a] TON is calculated per Co center and represents an average for all plateau values. The error corresponds to the standard deviation calculated for all plateau values.

[b] TOF is calculated as TON/h, given after 1 h. The error corresponds to the standard deviation for triplicate experiments.

## 5. Cyclic Voltammograms

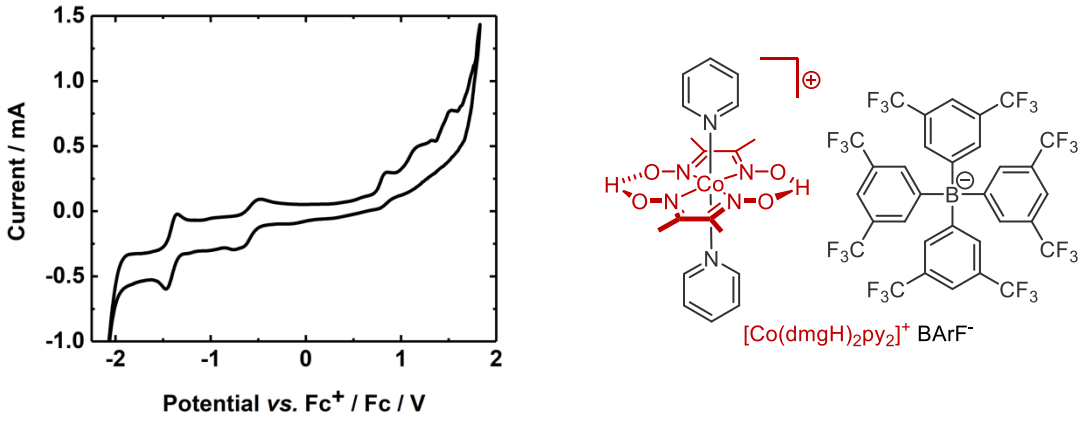


**Figure S2:** Cyclic voltammogram of $[Co(dmgH)_2(py)_2]^+BArF^-$ in acetonitrile. CV was recorded in acetonitrile at r.t., supporting electrolyte: $TBAPF_6$ (0.1 M), potentials *vs.* $Fc/Fc^+$. Scan rate 50 mV/s. [cobalt salt] = $1.0 \times 10^{-3}$ M.)

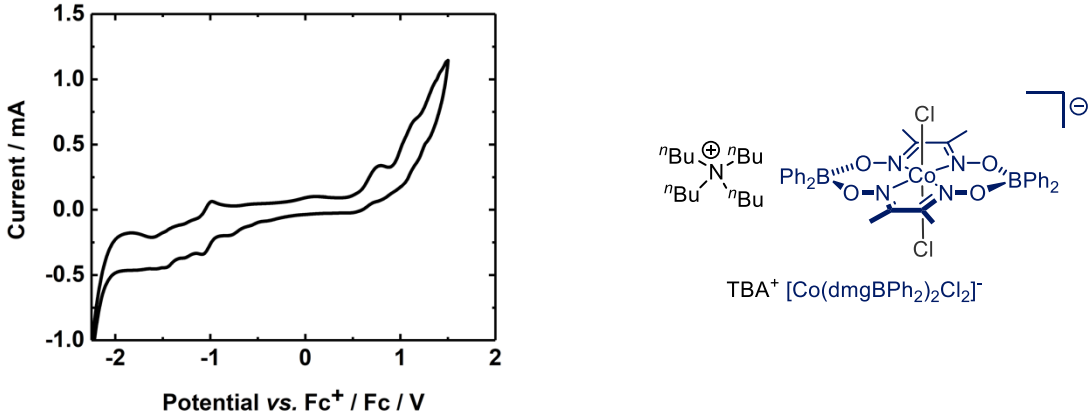


**Figure S3:** Cyclic voltammograms of $TBA^+[Co(dmgBPh_2)_2Cl_2]^-$ in acetonitrile. (CV was recorded in acetonitrile at r.t., supporting electrolyte: $TBAPF_6$ (0.1 M), potentials *vs.* $Fc/Fc^+$. Scan rate 50 mV/s. [cobalt salt] = $1.0 \times 10^{-3}$ M.)

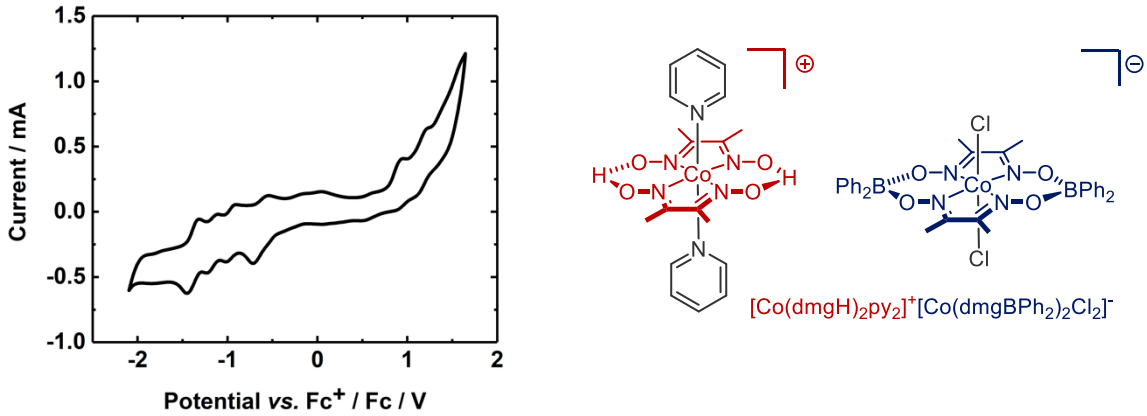


**Figure S4:** Cyclic voltammograms of $[Co(dmgH)_2(py)_2]^+[Co(dmgBPh_2)_2Cl_2]^-$ in acetonitrile. (CV was recorded in acetonitrile at r.t., supporting electrolyte: $TBAPF_6$ (0.1 M), potentials *vs.* $Fc/Fc^+$. Scan rate 50 mV/s. [cobalt salt] = $1.0 \times 10^{-3}$ M.)

The cyclovoltammograms showed insignificant changes during consecutive scans, especially regarding the important reductive peaks indicating their stability in the scanned potential window.

## 6. X-Ray Crystallographic Details

### 6.1. Comparison of Crystal Data of $[Co(dmgH)_2(py)_2]^+[Co(dmgBPh_2)_2Cl_2]^-$, and $[Co(dmgH)_2(py)Cl]$

**Table S3: Summary of bond lengths and angles in the solid state structure.[S3]**

| | $[Co(dmgH_2)_2(py)_2]^+[Co(dmgBPh_2)_2Cl_2]^-$ | | $[Co(dmgH)_2(py)Cl]$[S7] |
|---|---|---|---|
| | Cation | Anion | |
| distance Co-$N_a$ | 1.90 Å | 1.87 Å | 1.89 Å |
| distance Co-$N_b$ | 1.90 Å | 1.89 Å | 1.89 Å |
| distance Co-$N_{py}$ | 1.97 Å | - | 1.96 Å |
| distance Co-Cl | - | 2.24 Å | 2.23 Å |
| distance $N_a$-$O_a$ | 1.34 Å | 1.36 Å | 1.34 Å |
| distance $N_b$-$O_b$ | 1.35 Å | 1.37 Å | 1.35 Å |
| distance $O_a$-B | - | 1.52 Å | - |
| distance $O_b$-B | - | 1.51 Å | - |
| angle $N_a$-$O_a$-B | - | 115.7° | - |
| angle $N_b$-$O_b$-B | - | 116.4° | - |
| angle $N_a$-Co-$N_{py}$ | 89.1° | - | 90.6° |
| angle $N_b$-Co-$N_{py}$ | 89.5° | - | 89.9° |
| angle $N_a$-Co-Cl | - | 86.7° | 89.4° |
| angle $N_b$-Co-Cl | - | 87.1° | 89.9° |

The solid state structures of $[Co(dmgH)_2(py)_2]^+[Co(dmgBPh_2)_2Cl_2]^-$ and $[Co(dmgH)_2(py)Cl]$ are very similar in respect to most bond lengths and angles. Nevertheless, in the double complex salt, the chloride ligands deviate significantly from a 90° angle with the cobaloxime plane (compared to $[Co(dmgH)_2(py)Cl]$), which is very likely associated with steric constraints caused by the nearly parallelly oriented phenyl rings of $[Co(dmgBPh_2)_2Cl_2]^-$. This significant deviation from a 90° angle may be relevant for catalytic performance.

## 6.2. $[Co(dmgH)_2(py)_2]^+[Co(dmgBPh_2)_2Cl_2]^-$

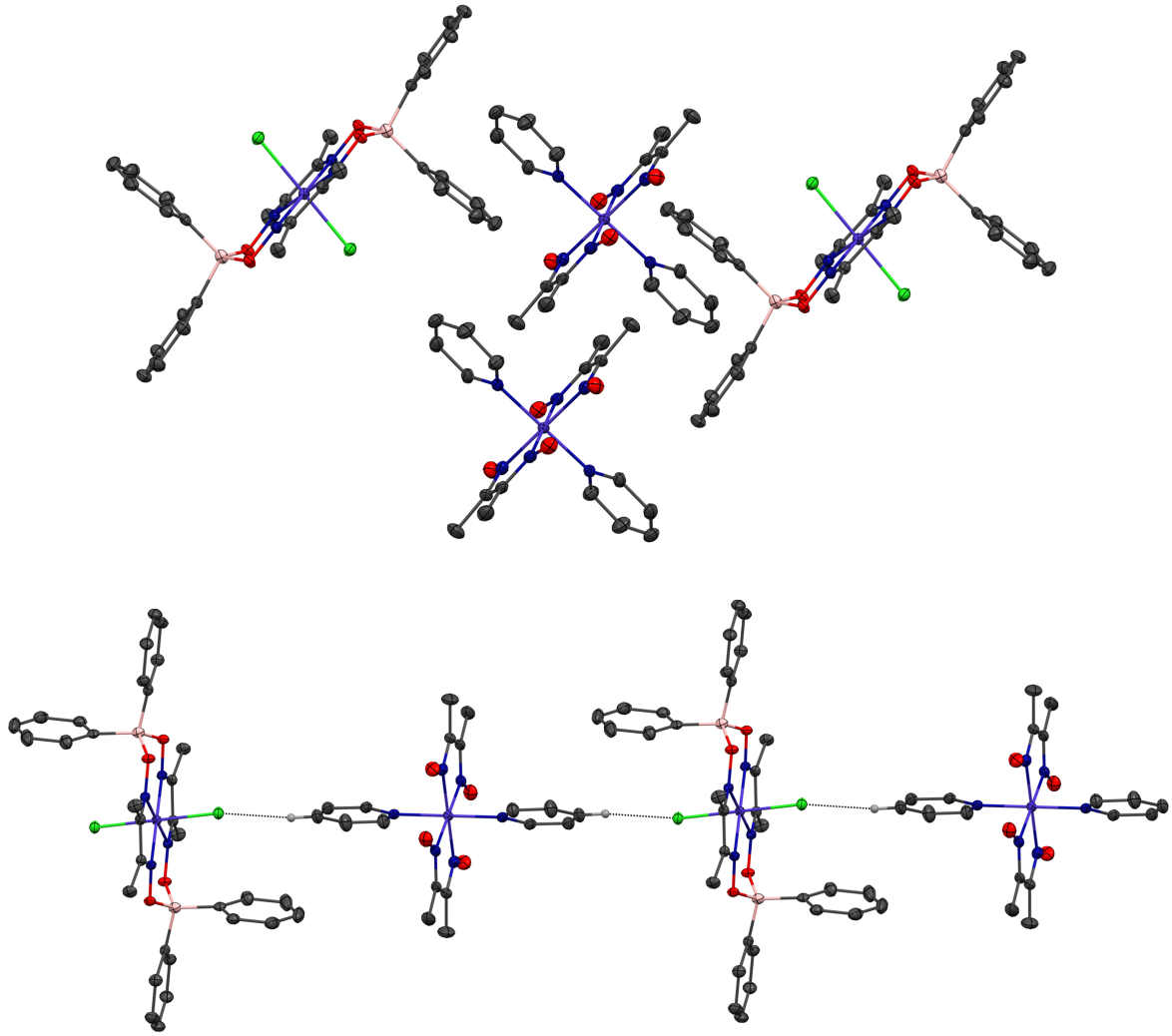

**Figure S5.** Graphical representations of the solid state structure of $[Co(dmgH)_2(py)_2]^+[Co(dmgBPh_2)_2Cl_2]^-$. Thermal ellipsoids are shown at the 50% probability level and hydrogen atoms were omitted for clarity. Top: General arrangement of $[Co(dmgH)_2(py)_2]^+$ and $[Co(dmgBPh_2)_2Cl_2]^-$. Bottom: $[Co(dmgH)_2(py)_2]^+[Co(dmgBPh_2)_2Cl_2]^-$ chain formation via short contact interactions between pyridine-based H-Atoms of $[Co(dmgH)_2(py)_2]^+$ and the Cl ligands of $[Co(dmgBPh_2)_2Cl_2]^-$ (short contacts are indicated as dashed lines and defined by: Distance between the two atoms is at least shorter by 0.1 Å than the sum of the atoms´ respective van der Waal´s radii). The cif-file was deposited in the Cambridge Structural Database under identifier CCDC 1958254.

**Table S4. Crystal data and structure refinement for $[Co(dmgH)_2(py)_2]^+[Co(dmgBPh_2)_2Cl_2]^-$**

| | |
|---|---|
| Empirical formula | $C_{25}H_{28}BClCoN_5O_4$ |
| Formula weight | 567.71 |
| Temperature/K | 149.95 |
| Crystal system | triclinic |
| Space group | P-1 |
| a/Å | 8.6168(5) |
| b/Å | 8.7453(6) |
| c/Å | 17.2091(10) |
| α/° | 83.882(5) |
| β/° | 87.942(5) |
| γ/° | 80.522(5) |
| Volume/Å$^3$ | 1271.61(14) |
| Z | 2 |
| $\rho_{calc}$g/cm$^3$ | 1.483 |
| μ/mm$^{-1}$ | 0.822 |
| F(000) | 588.0 |
| Crystal size/mm$^3$ | 0.143 × 0.083 × 0.078 |
| Radiation | MoKα (λ = 0.71073) |
| 2Θ range for data collection/° | 6.178 to 59.034 |
| Index ranges | -10 ≤ h ≤ 11, -11 ≤ k ≤ 11, -23 ≤ l ≤ 22 |
| Reflections collected | 11793 |
| Independent reflections | 6014 [$R_{int}$ = 0.0248, $R_{sigma}$ = 0.0425] |
| Data/restraints/parameters | 6014/0/345 |
| Goodness-of-fit on F$^2$ | 1.043 |
| Final R indexes [I>=2σ (I)] | $R_1$ = 0.0355, $wR_2$ = 0.0723 |
| Final R indexes [all data] | $R_1$ = 0.0477, $wR_2$ = 0.0795 |
| Largest diff. peak/hole / e Å$^{-3}$ | 0.40/-0.46 |

## 7. NMR Spectra

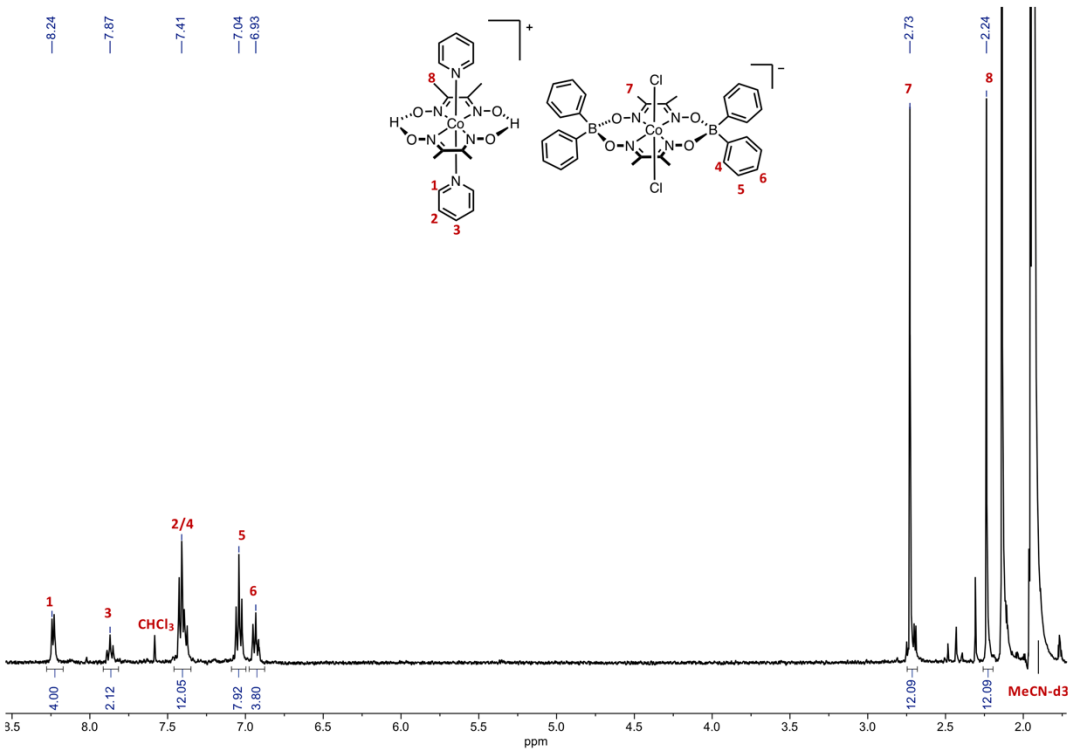


**Figure S6:** $^{1}$H-NMR spectrum (400 MHz, $CD_3CN$, 298 K) of $[Co(dmgH)_2(py)_2]^+[Co(dmgBPh_2)_2Cl_2]^-$. $H_2O$ impurity at 2.14 ppm and $CHCl_3$ impurity at 7.58 ppm.

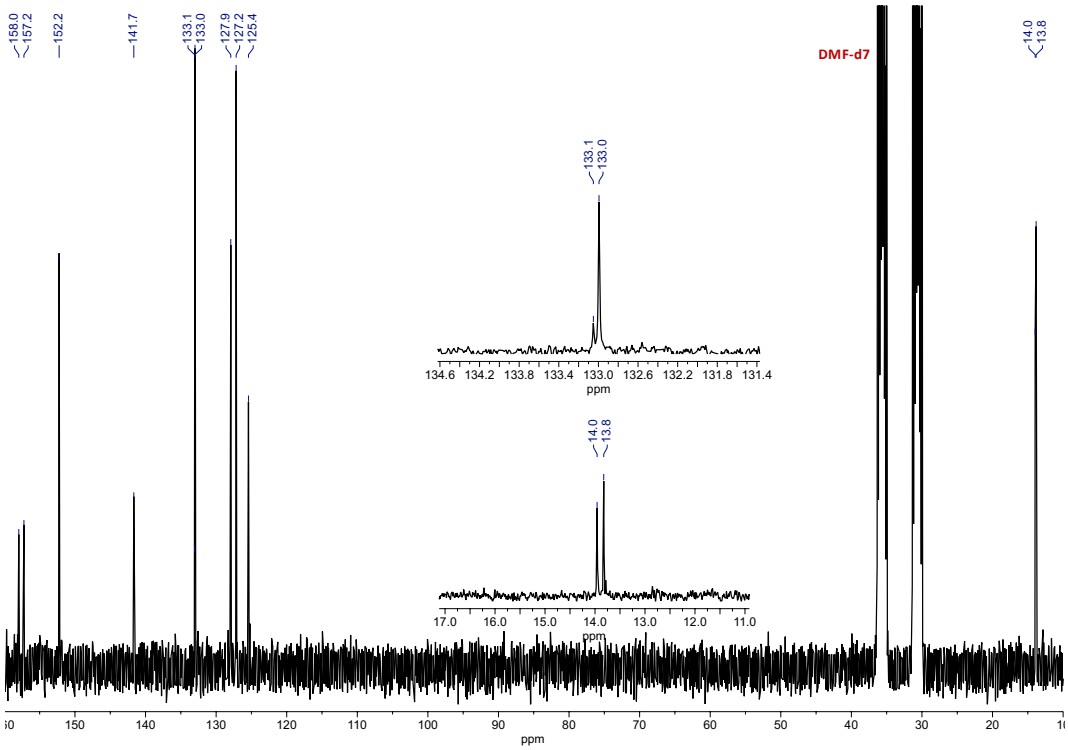


**Figure S7:** $^{13}$C-NMR spectrum (400 MHz, DMF-d7, 333 K) of $[Co(dmgH)_2(py)_2]^+[Co(dmgBPh_2)_2Cl_2]^-$.

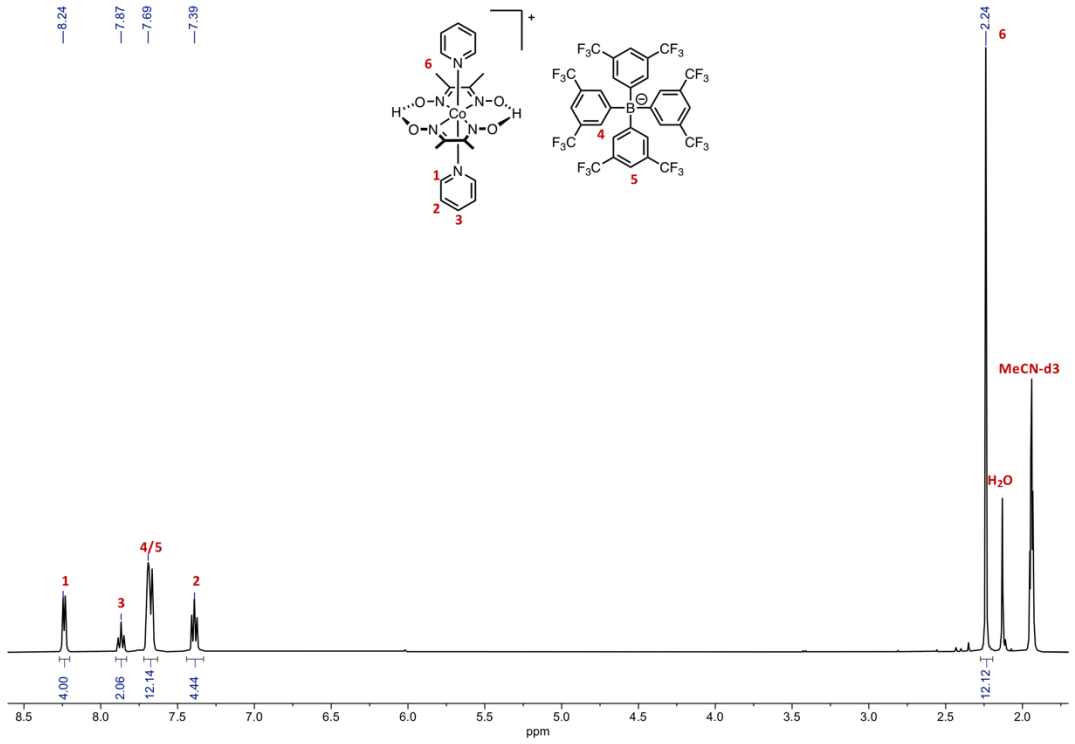


**Figure S8:** $^{1}$H-NMR spectrum (400 MHz, $CD_3CN$, 298 K) of $[Co(dmgH)_2(py)_2]^+$ $BArF^-$.

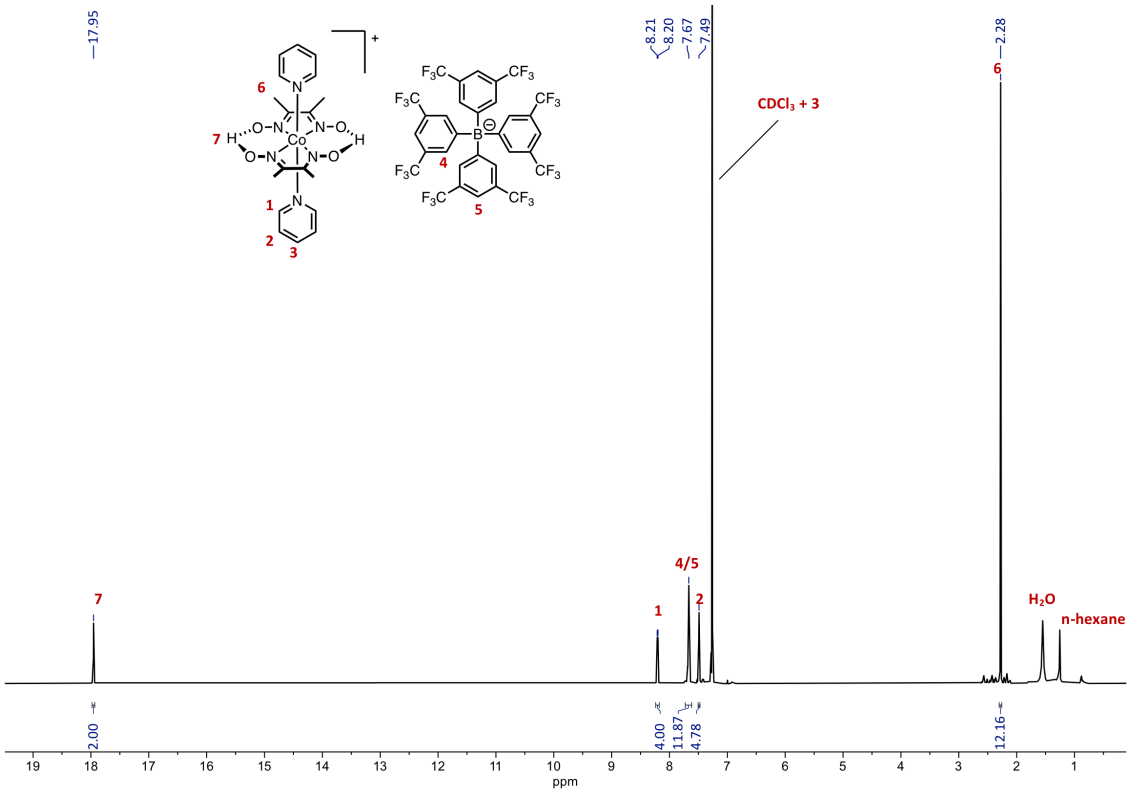


**Figure S9:** $^{1}$H-NMR spectrum (400 MHz, $CDCl_3$, 298 K) of $[Co(dmgH)_2(py)_2]^+$ $BArF^-$.

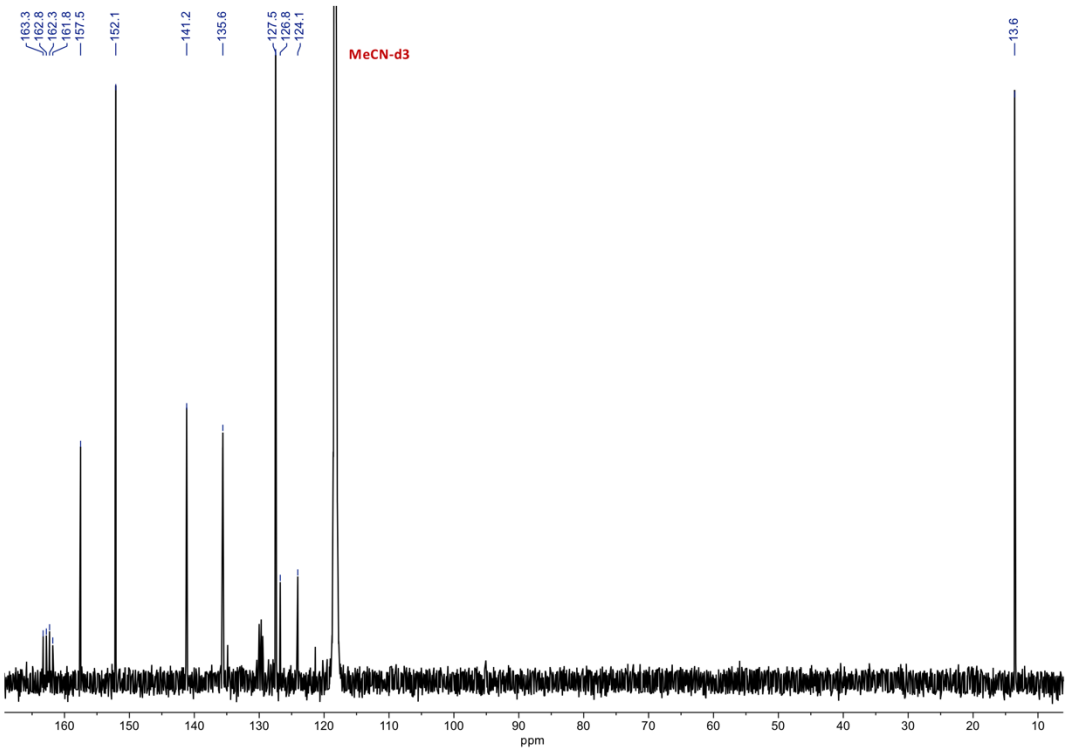


**Figure S10:** $^{13}$C-NMR spectrum (400 MHz, $CD_3CN$, 298K) of $[Co(dmgH)_2(py)_2]^+BarF^-$.

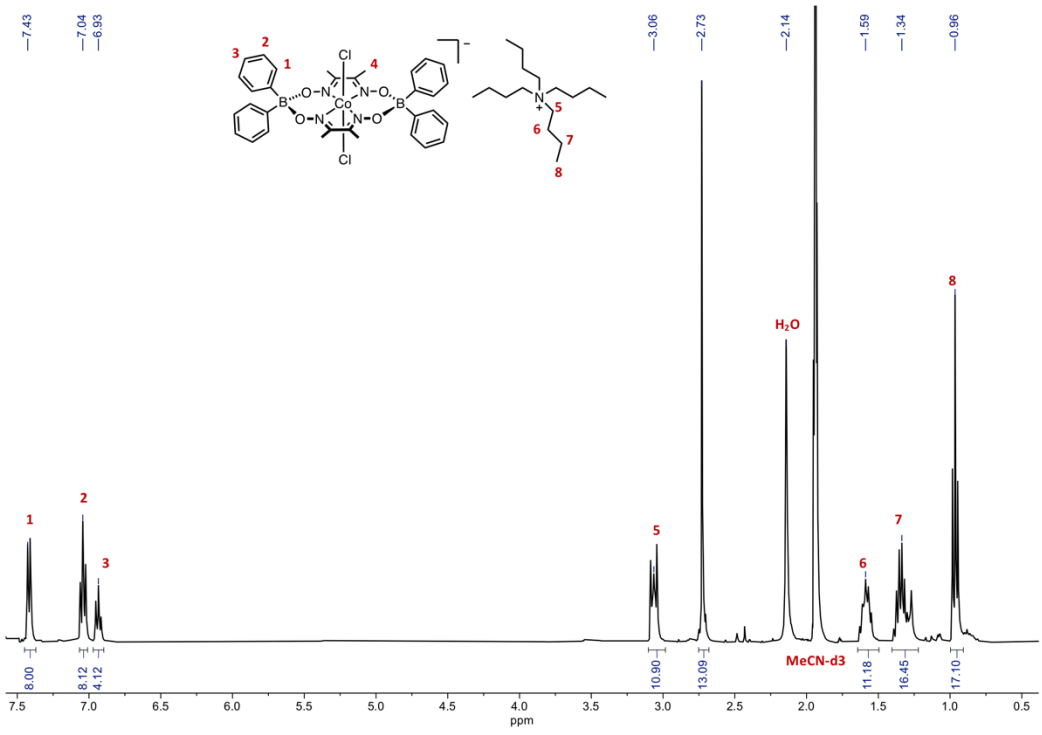


**Figure S11**: $^1$H-NMR spectrum (400 MHz, $CD_3CN$, 295 K) of $TBA^+$ $[Co(dmgBPh_2)_2Cl_2]^-$.

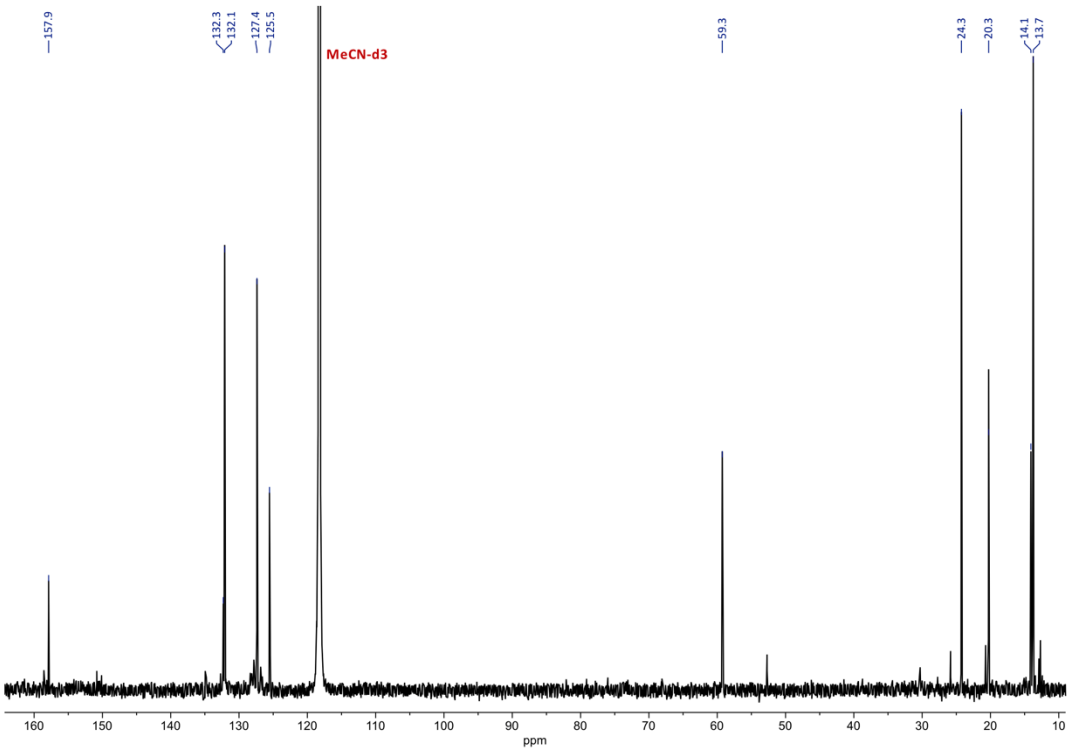


**Figure S12:** $^{13}$C-NMR spectrum (400 MHz, $CD_3CN$, 298K) of $TBA^+$ $[Co(dmgBPh_2)_2Cl_2]^-$.

## 8. Mass spectrometry

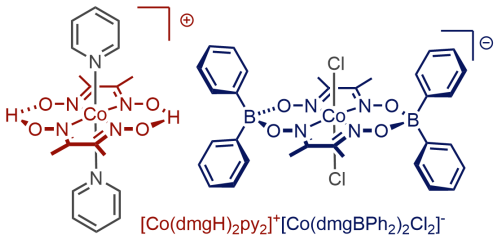


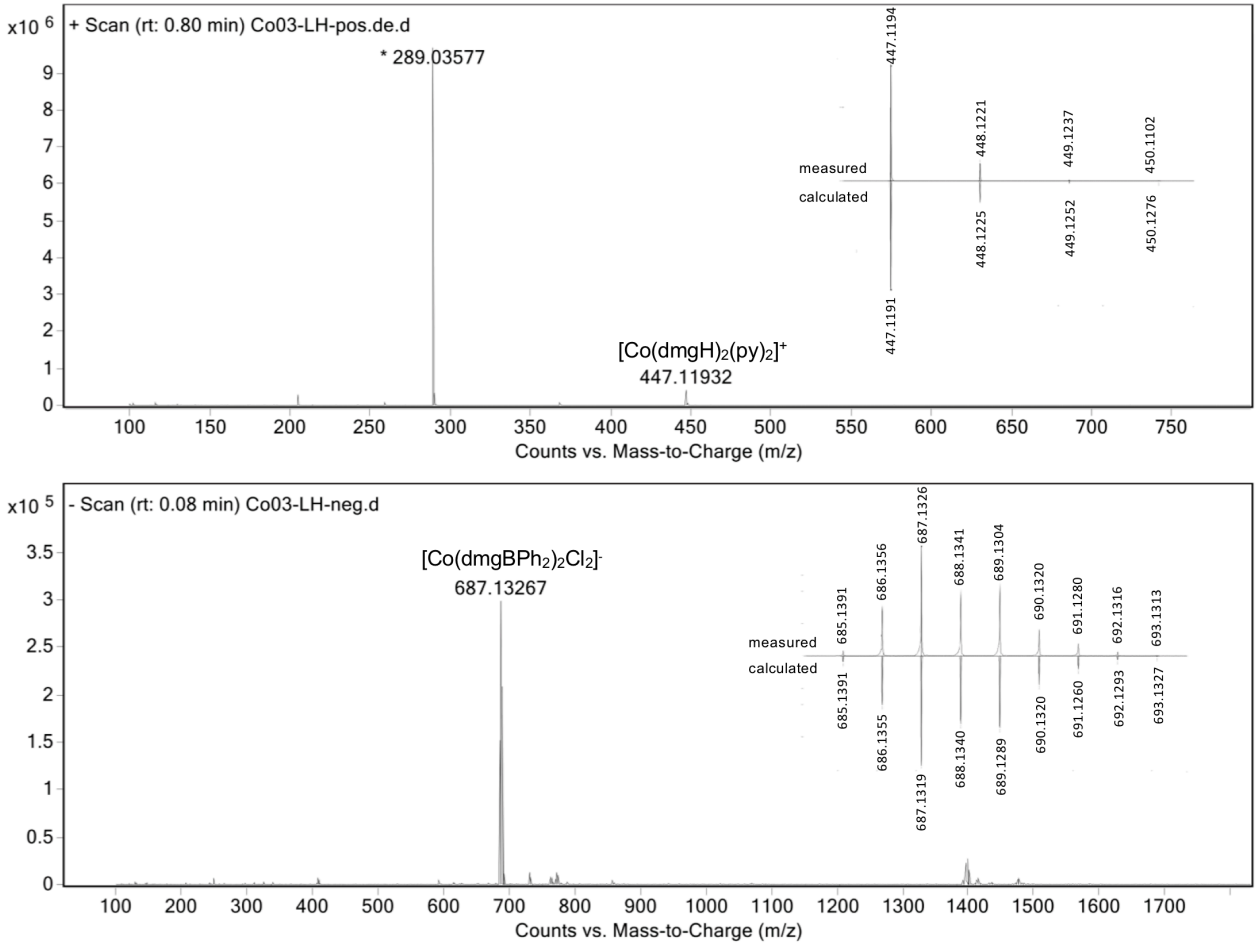


**Figure S13**: HR MS (ESI) of $[Co(dmgH)_2(py)_2]^+[Co(dmgBPh_2)_2Cl_2]^-$: a) positive mode (top): calculated for $C_{18}H_{24}CoN_6O_4$: 447.1191. Found: 447.1193. m/z: 289.03577 corresponds to $[Co(dmgH)_2]^+$; b) negative mode (bottom): Calculated for $C_{32}H_{32}B_2Cl_2CoN_4O_4$: 687.1319. Found: 687.1327.

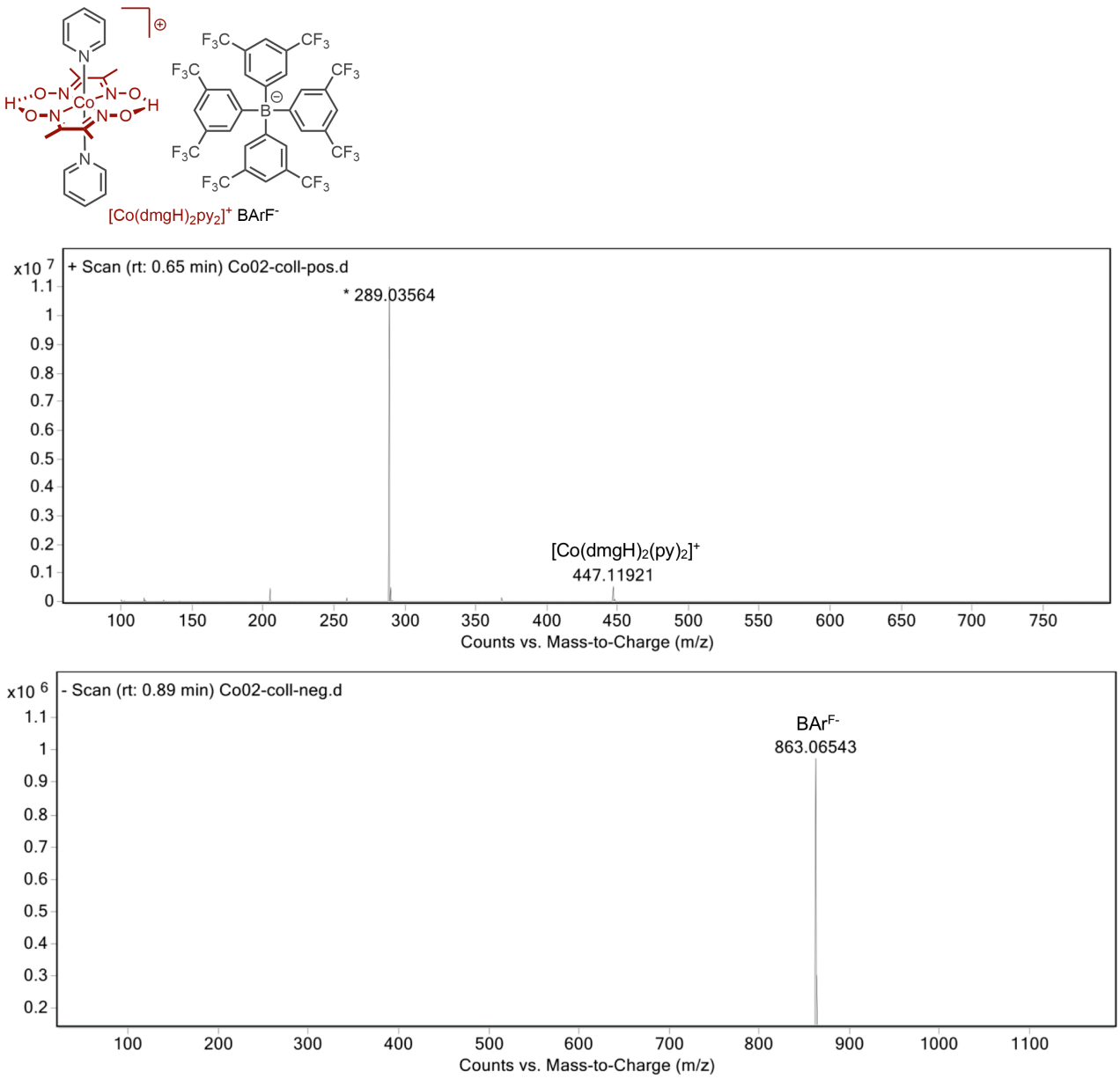


**Figure S14**: HR MS (ESI) of $[Co(dmgH)_2(py)_2]^+Bar^{F-}$: a) positive mode (top): calculated for $C_{18}H_{24}CoN_6O_4$: 447.1191. Found: 447.1192. m/z: 289.03564 corresponds to $[Co(dmgH)_2]^+$; b) negative mode (bottom): Calculated for $C_{32}H_{12}BF_{24}$: 863.0649. Found: 863.0654.

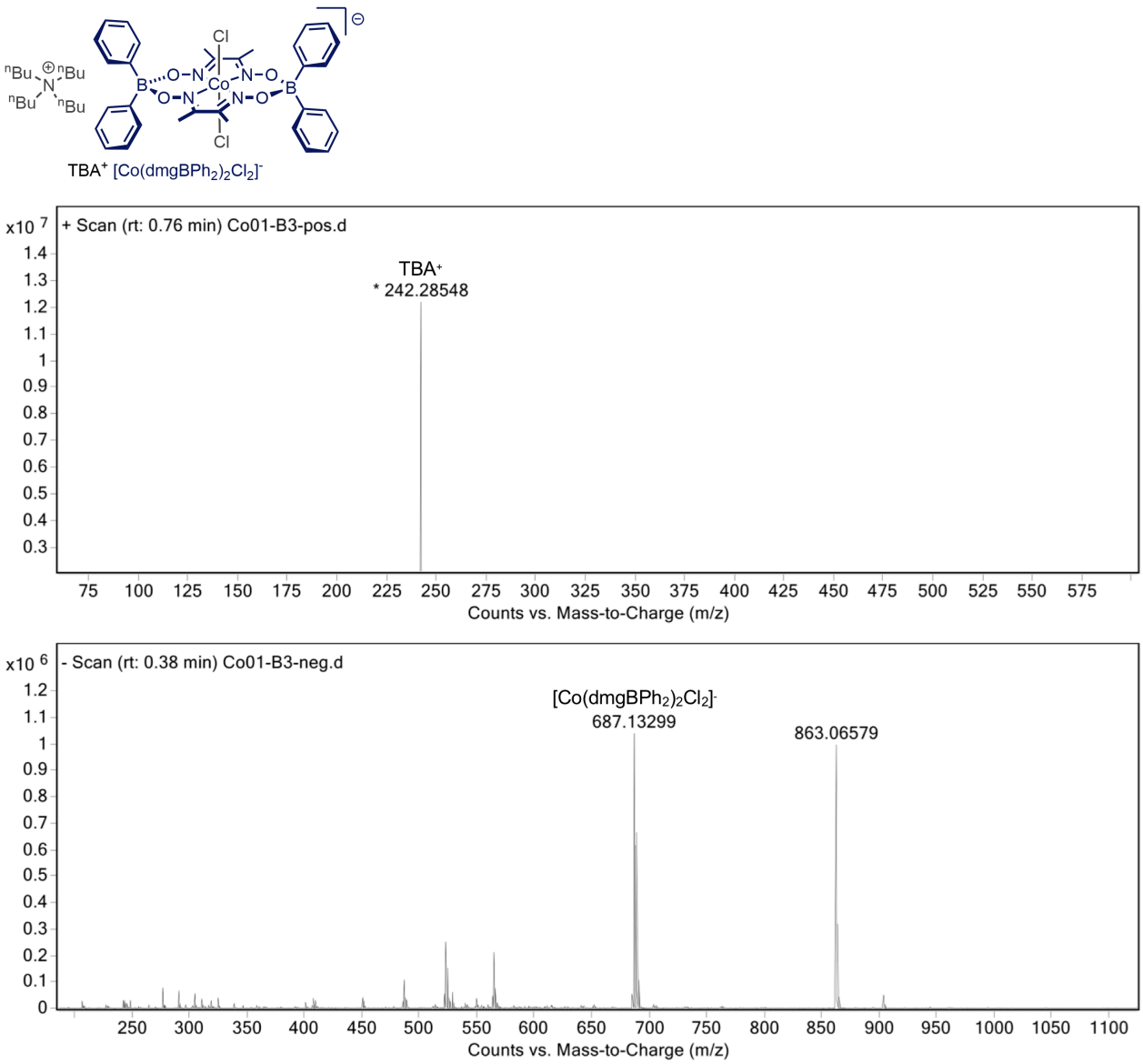


**Figure S15**: HR MS (ESI) of $TBA^+$ $[Co(dmgBPh_2)_2Cl_2]^-$: a) positive mode (top): calculated for $C_{16}H_{36}N$: 242.2848. Found: 242.28548; b) negative mode (bottom): Calculated for $C_{32}H_{32}B_2Cl_2CoN_4O_4$: 687.1319. Found: 687.13299. m/z: 863.06579 corresponds to $[BAr^F]^-$

## 9. SECCM Patterning

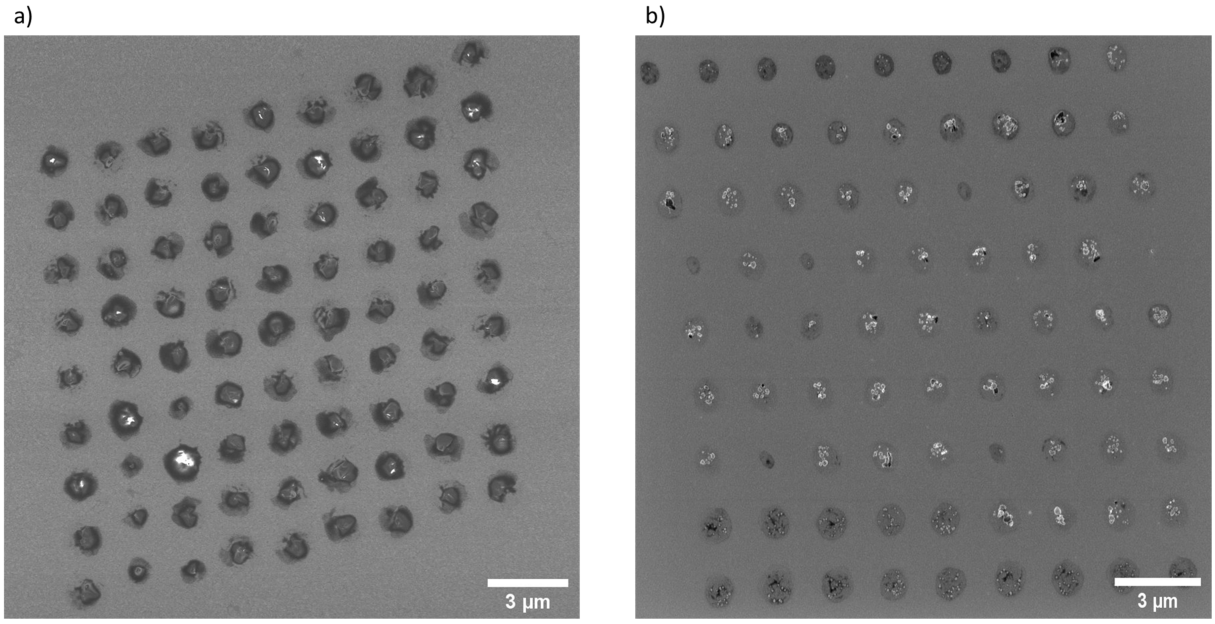


**Figure S16**: Representative SEM images of catalyst- modified of $NH_2$-CNM on Au substrate (area of 17 × 17 µm) with a) 81 spots of $[Co(dmgH)_2(py)_2]^+[Co(dmgBPh_2)_2Cl_2]^-$ (approx. spot diameter: 1 µm, spacing between spots: 1 µm) and b) with 81 spots of $[Co(dmgH)_2(py)Cl]$ (approx. spot diameter: 1 µm, spacing between spots: 1 µm). The micro-arrays were used for the proof-of-principle i*n-situ* $H_2$ measurements. Estimated area of active catalyst molecules: $[Co(dmgH)_2(py)_2]^+[Co(dmgBPh_2)_2Cl_2]^-$: 162.25 $\mu m^2$ (all 81 spots were included in calculation) and $[Co(dmgH)_2(py)Cl]$: 51.35 $\mu m^2$ (76 spots were included in the calculation) Estimations are based on assuming a hemispherical geometry of the spots and calculating the mantle of a hemisphere).

## 10. AFM Characterization

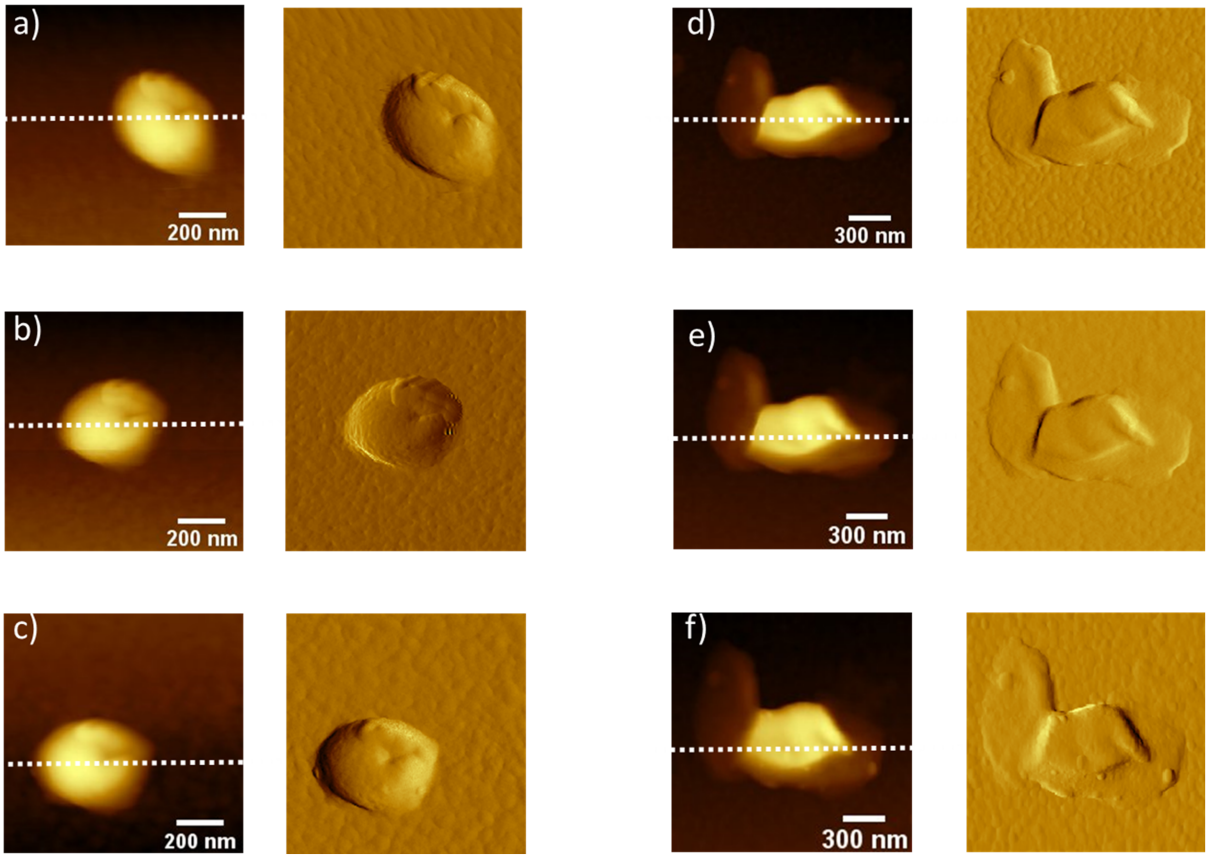


**Figure S17:** AFM contact mode topography (left) and deflection (right) images recorded in air: a) $[Co(dmgH)_2(py)_2]^+[Co(dmgBPh_2)_2Cl_2]^-$ spot deposited with a dual barrel nanopipette (overall orifice 400 nm) before illumination; b) same spot after 15 h of illumination in a solution containing 0.5 mM $[Ru(tbbpy)_2(mmip)]Cl_3$ and 0.1 M ascorbic acid (pH 4). c) the same spot after illuminating a second time for 15 h under the same conditions. d) $[Co(dmgH)_2(py)Cl]$ spot deposited with a dual barrel nanopipette (overall orifice 400 nm) before illumination; e) the same spot after 15 h of illumination in a solution containing 0.5 mM $[Ru(tbbpy)_2(mmip)]Cl_3$ and 0.1 M ascorbic acid (pH 4). c) the same spot after illuminating a second time for 15 h under the same conditions. All experiments were made in Ar purged solutions, overlaying the solutions with an Ar-stream for the duration of the illumination.

## 11. Characterization and positioning of $H_2$ Microsensor

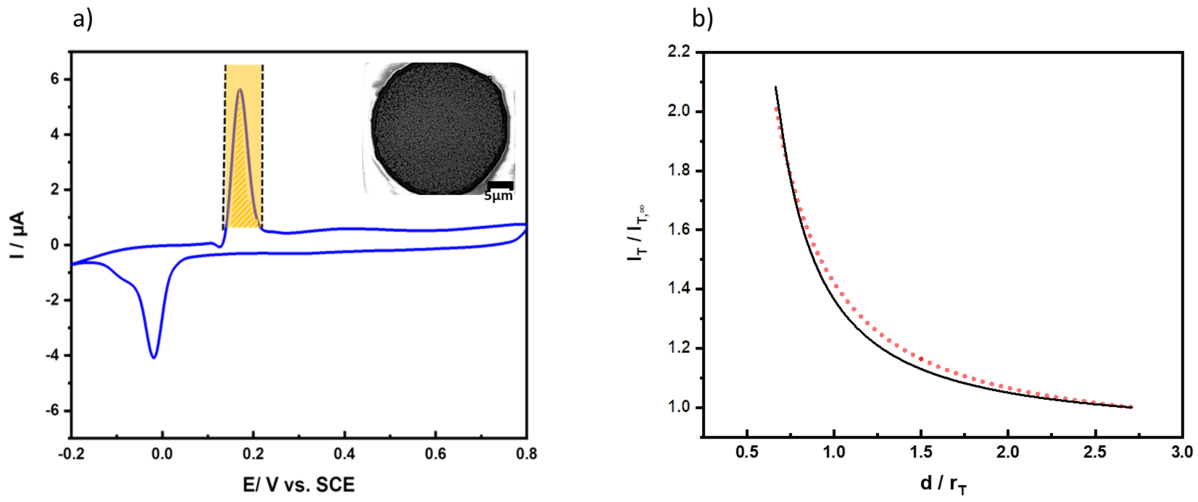


**Figure S18:** a) CV of a Pd-modified microelectrode recorded in de-aerated 0.5 M $H_2SO_4$ with a scan rate of 0.05 $V \cdot s^{-1}$. The cathodic peak at around -0.02 V shows the $H_2$ absorption and the anodic peak at approximately 0.2 V the oxidation of absorbed hydrogen. Inset: SEM image of a Pd-modified microelectrode with an active surface area of $5.0 \cdot 10^4$ $\mu m^2$ calculated from the recorded CVs.[S8] b) Exemplary SECM approach curve recorded in 5 mM 1,1'ferrocendimethanol /0.1 M KCl with a scan velocity 5 µm/s. Red dotted line is the experimental curve showing positive feedback current; black solid line is the theoretical approach curve using the fitting approach of Amphlett and Denuault.[S9]

## 12. Control experiments

### 12.1. Stability studies of the $Co(dmgH)_2(py)Cl]$ catalyst

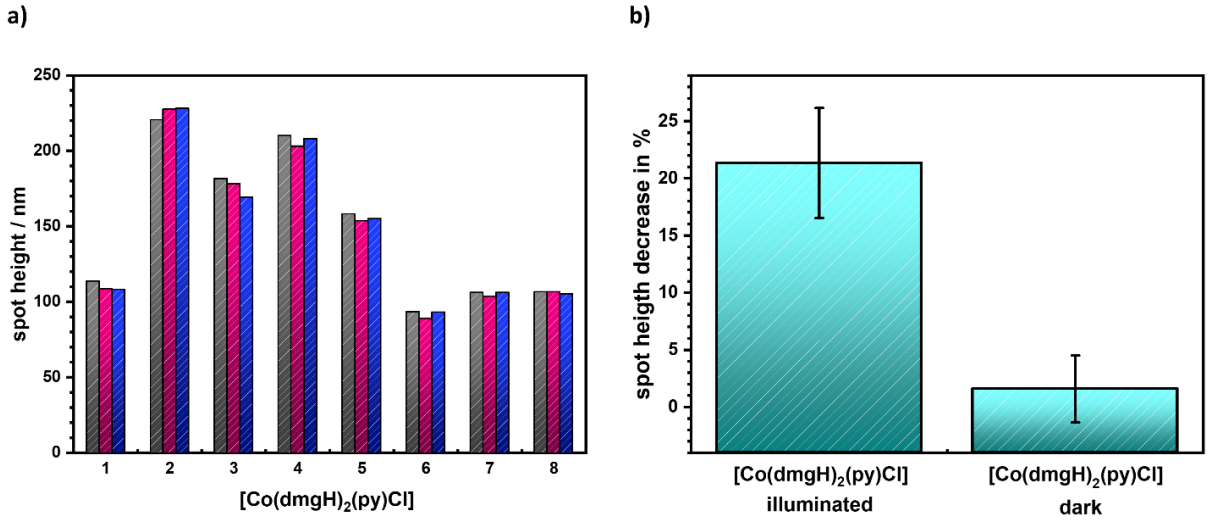


**Figure S19:** Control experiment for $[Co(dmgH)_2(py)Cl]$ stability: The $[Co(dmgH)_2(py)Cl]$ spots were stored under dark conditions in 0.5 mM $[Ru(tbbpy)_2(mmip)]Cl_3$ and 0.1 M ascorbic acid solution (pH 4) two times for 15 hours (in total 30 hours of immersion). a) Bar diagram of the average height decrease in dependence of time for 8 spots (determined via contact mode AFM) of $[Co(dmgH)_2(py)Cl]$ before (grey), after 15 h (red) and after 30 h stored in the reaction solution. b) Bar diagram of the height decrease in percentage in after 30 h of the illuminated and the non-illuminated spots. All experiments were performed in an Ar purged solutions and under Ar-atmosphere.

## 12.2. Control experiments for in-situ $H_2$ measurements

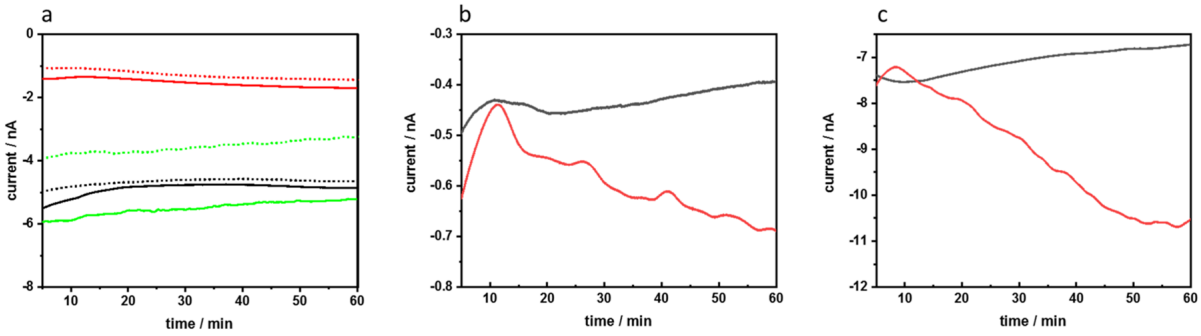


**Figure S20:** Control experiments for the in-situ $H_2$ measurements: a) amperometric I-t curves with only 0.1 M ascorbic acid in solution (black lines), with only 0.5 mM $[Ru(tbbpy)_2(mmip)][Cl_3]$ in solution (red lines) and with 0.1 M ascorbic acid and 0.5 mM $[Ru(tbbpy)_2(mmip)]Cl_3$ (pH 4) (green lines). Measurements were recorded with a Pd microsensor positioned over a $[Co(dmgH)_2(py)_2]^+[Co(dmgBPh_2)_2Cl_2]^-$ microarray (black and red lines) or over a bare Au substrate (green lines). Dotted lines show the measurements under dark conditions and solid lines under illumination. All experiments were performed under argon atmosphere. b) Amperometric I-t curves of $H_2$ measurement at a $[Co(dmgH)_2(py)Cl]$ microarray in 0.5 mM $[Ru(tbbpy)_2(mmip)]Cl_3$ and 0.1 M ascorbic acid (pH 4) (black line in dark condition; red line under illumination. c) Amperometric I-t curves of a $H_2$ measurement at a $[Co(dmgH)_2(py)_2]^+[Co(dmgBPh_2)_2Cl_2]^-$ microarray in 0.5 mM $[Ru(tbbpy)_2(mmip)]Cl_3$ and 0.1 M ascorbic acid (pH 4) (black line in dark condition; red line under illumination). A potential of -0.6 V vs Ag/AgCl was applied at the Pd-microelectrode.

## 12.3. pH dependence of HER performance at $[Co(dmgH)_2(py)Cl]$ microarrays

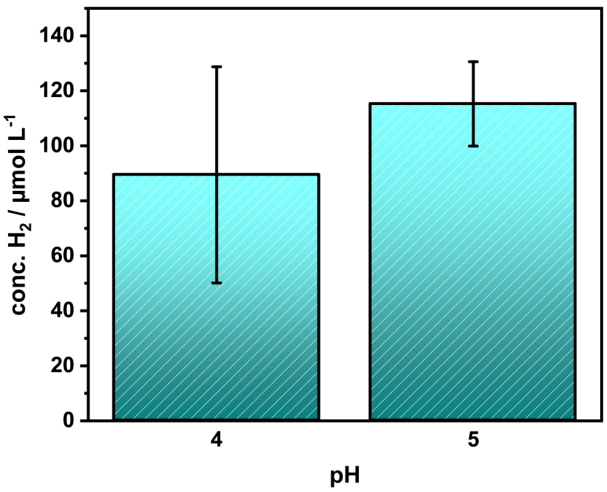


**Figure S21:** Comparison of the $H_2$ measurement at $[Co(dmgH)_2(py)Cl]$ spots in solutions with pH 4 and pH 5: The bar diagrams show the $H_2$ concentration after one hour illumination at a $[Co(dmgH)_2(py)Cl]$ microarray in 0.5 mM $[Ru(tbbpy)_2(mmip)]Cl_3$ and 0.1 M ascorbic acid at pH 4 (n = 3) and pH 5 (n = 3), respectively.

## 13. References


[S1] S. Kaufhold, L. Petermann, D. Sorsche, S. Rau, *Chem. Eur. J.* **2017**, *23*, 2271–2274.

[S2] A. Fihri, V. Artero, M. Razavet, C. Baffert, W. Leibl, M. Fontecave, *Angew. Chemie Int. Ed.* **2008**, *47*, 564–567.

[S3] O. V. Dolomanov, L. J. Bourhis, R. J. Gildea, J. A. K. Howard, H. Puschmann, *J. Appl. Cryst.* **2009**, *42*, 339–341.

[S4] G. M. Sheldrick, *Acta Cryst.* **2008**, *A64*, 112–122.

[S5] G. M. Sheldrick, G.M. *Acta Cryst.* **2008**, *C71*, 3–8.

[S6] C. F. Macrae, P. R. Edgington, P. McCabe, E. Pidcock, G. P. Shields, R. Taylor, M. Towler, J. van de Streek, *J. Appl. Cryst.* **2006**, *39*, 453–457.

[S7] S. Geremia, R. Dreos, L. Randaccio, G. Tauzher, L. Antolini, *Inorg. Chim. Acta* **1994**, *216*, 125–129.

[S8] A. N. Correia, L. H. Mascaro, S. A. S. Machado, L. A. Avaca, *Electrochim. Acta* **1997**, *42*, 493–495.

[S9] J. A. Amphlett, G. Denuault, *J. Phys. Chem. B* **1998**, *102*, 9946–9951.